Phenomenological modeling of shape memory alloy thermomechanical behavior

Marcelo A. Savi
Universidade Federal do Rio de Janeiro, COPPE - Department of Mechanical Engineering, Rio de Janeiro, RJ – Brazil
Alberto Paiva
Universidade Federal Fluminense, Escola de Engenharia Industrial Metalúrgica de Volta Redonda, Volta Redonda, RJ – Brazil
Pedro Manuel C. L. Pacheco
CEFET/RJ - Department of Mechanical Engineering, Rio de Janeiro, RJ – Brazil

Abstract

Shape memory alloys (SMAs) remarkable properties have attracted much technological interest in many research fields in the last decades. Despite of being widely used in many applications, their constitutive modeling is still in focus for many researchers due to their great variety of complex behaviors. Although many efforts towards SMAs' thermomechanical behavior correct description has been done so far, it is common to find both simple models that are able to describe the main simple phenomena and more sophisticated models that are able to describe only a single complex phenomenon. Within this context, this article presents a one-dimensional macroscopic constitutive theory with internal constraints, which describes SMAs thermomechanical behavior, accounting for plasticity, plastic-phase transformation coupling, tension-compression asymmetry and transformation induced plasticity. Comparisons between experimental data found in the literature and numerical results provided by the model attest its capability to capture, besides the basic phenomena, more advanced features concerning SMAs' behavior.

Keywords: shape memory alloy, constitutive modeling, transformation induced plasticity, plastic-phase transformation coupling, tension-compression asymmetry.

1 Introduction

Shape Memory Alloys (SMAs) are metallic compounds able to recover their original shape (or to develop meaningful forces when they have their recovery constrained) when subjected to a temperature and/or a stress field, due to phase transformations the material undergoes.

Brazilian Society of Mechanical Sciences and Engineering, ISBN 978-85-85769-30-7

This class of materials is usually applied as actuators in the so-called intelligent structures for their adaptive behavior according to its environment. Biomedical applications have obtained a great success due to SMAs' functional properties, increasing the performance of less invasive surgeries. The biocompatibility of these alloys plays an important role in biomedical applications [1, 2]. They are also ideally suited for non-medical applications such as self-actuating fasteners, thermally activated actuator switches, self-expanding washers, smart clamps, among other possibilities [3–5]. The use of SMAs can help solving important problems in aerospace technology, for instance: self-erectable structures or non-explosive release devices that ensure satellite panels opening [6, 7]. SMA micromanipulators and robotics actuators are built to mimic the smooth motions of human muscles [8–10]. Moreover, they are being used as actuators for vibration and buckling control of flexible structures. In this particular case, SMA wires are usually embedded in a composite element to modify mechanical properties of slender structures [10, 11]. The main drawback of SMAs is that, since they are thermally actuated, they present a slow actuation rate compared with electrically actuated devices.

SMAs present complex thermomechanical behaviors related to different physical processes. Besides the most common phenomena presented by this class of materials, such as pseudoelasticity, shape memory effect, which may be one-way (SME) or two-way (TWSME) and phase transformation due to temperature variation, there are more complicated phenomena that have significant influence over its overall thermomechanical behavior, for instance: plastic behavior, plastic-phase transformation coupling, tension-compression asymmetry, transformation induced plasticity (TRIP), among others. All these phenomena take place at a microscopic level but most of them affect SMAs' macroscopic response; therefore, they should not be neglected while modeling their phenomenological behavior.

SMAs thermomechanical behavior can be modeled either by microscopic (interested in metallurgical features) or by macroscopic (interested in phenomenological features) points of view. There is also an intermediate mesoscopic approach, interested in the lattice of the particles. Paiva & Savi [5] present an overview of constitutive models for SMAs thermomechanical description.

The phenomenological model presented in this contribution is a one-dimensional macroscopic constitutive model built upon Fremond's theory [12, 13]. The original model was developed for a three-dimensional media, being able to reproduce both pseudoelasticity and shape memory effect, with the aid of three internal variables that should obey internal constraints related to the coexistence of the different phases. The modified model takes into account some changes in the original formulation that allow new phenomena description such as linear hardening plasticity, plastic-phase transformation coupling, phase transformation due to temperature variation, internal subloops due to incomplete phase transformation, tension-compression asymmetry and transformation induced plasticity (TRIP). Each evolution step of the model here presented has been reported before in different references [5, 14–18]. The main goals of this work are to summarize the most interesting information about the theory and to present a collection of results provided by the model, comparing them with experimental results found in the literature.

Mechanics of Solids in Brazil 2007, Marcílio Alves & H.S. da Costa Mattos (Editors)
Brazilian Society of Mechanical Sciences and Engineering, ISBN 978-85-85769-30-7

2 Constitutive model

The proposed model formulation considers four volumetric fractions related to macroscopic phases: β_1 is associated with tensile detwinned martensite ($M+$), β_2 is related to compressive detwinned martensite (M–), β_3 represents austenite (A) and β_4 corresponds to twinned martensite (M). A Helmholtz free energy potential (ψ) is adopted for each individual phase, considering four state variables: elastic strain (ε_e), temperature (T) and two internal variables (γ and μ) that help the plastic phenomenon description, which are associated with the isotropic and kinematic hardening, respectively.

$$M+: \rho\ \psi_1\ (\varepsilon_e, T, \gamma, \mu) = \frac{1}{2} E_M\, \varepsilon_e^2 - \alpha^T \varepsilon_e - \Lambda_M^T - \Omega_M\ (T - T_0)\ \varepsilon_e + \frac{1}{2} K_M\, \gamma^2 + \frac{1}{2\, H_M} \mu^2 \tag{1}$$

$$M--: \rho\ \psi_2\ (\varepsilon_e, T, \gamma, \mu) = \frac{1}{2} E_M\, \varepsilon_e^2 + \alpha^C \varepsilon_e - \Lambda_M^C - \Omega_M\ (T - T_0)\ \varepsilon_e + \frac{1}{2} K_M\, \gamma^2 + \frac{1}{2\, H_M} \mu^2 \tag{2}$$

$$A: \rho\ \psi_3\ (\varepsilon_e, T, \gamma, \mu) = \frac{1}{2} E_A\, \varepsilon_e^2 - \Lambda_A - \Omega_A\ (T - T_0)\ \varepsilon_e + \frac{1}{2} K_A\, \gamma^2 + \frac{1}{2\, H_A} \mu^2 \tag{3}$$

$$M: \rho\ \psi_4\ (\varepsilon_e, T, \gamma, \mu) = \frac{1}{2} E_M\, \varepsilon_e^2 + \Lambda_M - \Omega_M\ (T - T_0)\ \varepsilon_e + \frac{1}{2} K_M\, \gamma^2 + \frac{1}{2\, H_M} \mu^2 \tag{4}$$

In the previous equations, subscript M is related to martensitic phase while A is associated with austenite. Moreover, superscript T is related to tensile parameters while C is associated with compressive parameters. Observing these indexes, notice that α's are material parameters related to phase transformation, while Λ's are associated with phase transformations stress levels and are temperature dependent (as will be later discussed); E's represent the elastic moduli, Ω's are related to the thermal expansion coefficients, K's are the plastic modulus while H's are the kinematic hardening moduli; T_0 is a reference temperature and ρ is the density.

Here, four more state variables should be added to express the free energy of the whole mixture ($\tilde{\psi}$), which is written weighting each energy potential with the corresponding volumetric fraction. Obviously, it is possible to consider only three volumetric fractions, since $\beta_1 + \beta_2 + \beta_3 + \beta_4 = 1$. Therefore, the total free energy is given by:

$$\rho\ \psi\ (\varepsilon_e,\ T,\ \gamma,\ \mu,\ \beta_i, \xi_i) = \rho\ \tilde{\psi}\ (\varepsilon_e,\ T,\ \gamma,\ \mu,\ \beta_i) +\ J_\pi\ (\beta_i) +\ J_\tau\ (\xi_i) \tag{5}$$

where $J_\pi\ (\beta_i)$ is the indicator function of the convex set π, which establishes the constraints associated to the phases' coexistence defined as follows. From now on, the subscript index i refers to i = 1,2,3 ($M+$, $M-$ and A, respectively).

$$\pi = \{\, \beta_i \in \Re \mid 0 \le \beta_i \le 1;\ \ \beta_1 + \beta_2 + \beta_3 \le 1 \,\} \tag{6}$$

while $J_\tau\ (\xi_i)$ is the indicator function associated with the constraints related to saturation effect during cyclic loadings according to the following relations, where ξ_i are the internal variables associated with

TRIP, m_i are saturation parameters ,while $\bar{M}$'s give the magnitude of TRIP deformation.

$$M_{13} = \bar{M}_{13} \exp\,(-m_1\,\xi_1)\,; \quad M_{31} = \bar{M}_{31} \exp\,(-m_1\,\xi_1) \tag{7}$$

Analogous expressions are used for $\bar{M}_{23}$, $\bar{M}_{32}$, $\bar{M}_{34}$ and $\bar{M}_{43}$. In order to control the amount of TRIP deformation at different temperatures, ε_{tp} should be temperature dependent as well. Thus, the parameters $\bar{M}_{13}$, $\bar{M}_{31}$, $\bar{M}_{23}$ and $\bar{M}_{32}$ are assumed to be linearly dependent on temperature. For instance, for $\bar{M}_{13}$, the following expression is adopted.

$$\begin{cases} \bar{M}_{13} = 0 \text{ if } T < T_{TRIP} \\ \bar{M}_{13} = \bar{M}_{13}^{Ref}\,\frac{(T - T_{TRIP})}{T_F - T_{TRIP}} \text{ if } T \geq T_{TRIP} \end{cases} \tag{8}$$

where $\bar{M}_{13}^{Ref}$ is a reference value of $\bar{M}_{13}$ at $T = T_F$ and T_{TRIP} is the temperature below which no transformation plasticity should exists. Analogous expressions are used for $\bar{M}_{31}$, $\bar{M}_{23}$ and $\bar{M}_{32}$.

After this, it is assumed an additive decomposition such that the elastic strain may be written as: $\varepsilon_e = \varepsilon - \varepsilon_p - \varepsilon_{tp} + \alpha_h^C \beta_2 - \alpha_h^T \beta_1$. Here, ε_p represents the plastic strain, ε_{tp} is associated to the TRIP deformation and ε is the total strain, while α_h's are material parameters related to phase transformation. As a result, the total free energy in its final form is expressed by:

$$\begin{aligned}
&\rho\ \psi\ (\varepsilon, \varepsilon_p, \varepsilon_{tp}, T,\ \gamma,\ \mu,\ \beta_i, \xi_i) = \beta_1 \left[-\alpha^T \left(\varepsilon - \varepsilon_p - \varepsilon_{tp} + \alpha_h^C \beta_2 - \alpha_h^T \beta_1 \right) - (\Lambda_M + \Lambda_M^T) \right] + \\
&+ \beta_2 \left[\alpha^C \left(\varepsilon - \varepsilon_p - \varepsilon_{tp} + \alpha_h^C \beta_2 - \alpha_h^T \beta_1 \right) - (\Lambda_M + \Lambda_M^C) \right] + \\
&+ \beta_3 \left[\frac{1}{2}\,(E_A - E_M) \left(\varepsilon - \varepsilon_p - \varepsilon_{tp} + \alpha_h^C \beta_2 - \alpha_h^T \beta_1 \right)^2 - (\Lambda_A + \Lambda_M) - \right. \\
&\left. - (\Omega_A - \Omega_M)\ (T - T_0) \left(\varepsilon - \varepsilon_p - \varepsilon_{tp} + \alpha_h^C \beta_2 - \alpha_h^T \beta_1 \right) + \frac{1}{2}\,(K_A - K_M)\ \gamma^2 + \left(\frac{1}{2\,H_A} - \frac{1}{2\,H_M} \right)\ \mu^2 \right] + \\
&+ \frac{1}{2} E_M \left(\varepsilon - \varepsilon_p - \varepsilon_{tp} + \alpha_h^C \beta_2 - \alpha_h^T \beta_1 \right)^2 + \Lambda_M - \Omega_M\ (T - T_0) \left(\varepsilon - \varepsilon_p - \varepsilon_{tp} + \alpha_h^C \beta_2 - \alpha_h^T \beta_1 \right) + \\
&+ \frac{1}{2} K_M\,\gamma^2 + \frac{1}{2\,H_M} \mu^2 + \ J_\pi\,(\beta_i) + \ J_\tau\,(\xi_i)
\end{aligned} \tag{9}$$

The state equations can be obtained from the Helmholtz free energy as follows:

$$\sigma = \rho\,\frac{\partial\,\psi}{\partial\,\varepsilon} \quad B_i \in -\rho\frac{\partial \psi}{\partial \beta_i} \quad X = -\rho\frac{\partial\,\psi}{\partial\,\varepsilon_p} = \sigma \quad Y = -\rho\frac{\partial\,\psi}{\partial\,\gamma} \quad Z = -\rho\frac{\partial\,\psi}{\partial\,\mu}$$

$$R = -\rho\frac{\partial\,\psi}{\partial\,\varepsilon_{tp}} = \sigma \quad S_i \in -\rho\,\frac{\partial \psi}{\partial \xi_i} \tag{10}$$

where the thermodynamic forcesB_i are associated with β_i; X, Y and Z are related to the classical plasticity phenomenon and R and S_i correspond to the TRIP effect. σ represents the uniaxial stress.

Mechanics of Solids in Brazil 2007, Marcílio Alves & H.S. da Costa Mattos (Editors)
Brazilian Society of Mechanical Sciences and Engineering, ISBN 978-85-85769-30-7

In order to describe the dissipation processes, it is necessary to introduce a pseudo-potential of dissipation Φ. In general, it is possible to split Φ into an intrinsic part (ϕ) and a thermal part (ϕ_T) as follows:

$$\Phi = \Phi\left(\dot{\varepsilon}, \dot{\varepsilon}_p, \dot{\varepsilon}_{tp},\ \dot{\gamma},\ \dot{\mu},\ \dot{\beta}_i, \dot{\xi}_i, q\right) = \phi\left(\dot{\varepsilon}, \dot{\varepsilon}_p, \dot{\varepsilon}_{tp},\ \dot{\gamma},\ \dot{\mu},\ \dot{\beta}_i, \dot{\xi}_i\right) + \phi_T(q) \tag{11}$$

Here, the interest is focused on the mechanical part of the potential and, for convenience, it is expressed in terms of its dual (ϕ^*).

$$\begin{aligned}\phi^*\left(B_i, X, Y, Z, R, S_i\right) = {} & \frac{1}{2\eta_1}\left(B_1 + \eta_{ci} Y + \eta_{ck} Z\right)^2 + \frac{1}{2\eta_2}\left(B_2 + \eta_{ci} Y + \eta_{ck} Z\right)^2 + \\ & + \frac{1}{2\eta_3}\left(B_3 - \eta_{ci} Y - \eta_{ck} Z\right)^2 + R^2\left[\left(M_{13}\beta_1 + M_{31}\beta_3\right)\dot{\beta}_1 + \left(M_{23}\beta_2 + M_{32}\beta_3\right)\dot{\beta}_2\right] + \\ & + R\ \left[M_{34}\beta_3 + M_{43}\left(1 - \beta_1 - \beta_2 - \beta_3\right)\right]\ \dot{\beta}_3 + \left|\dot{\beta}_1\right|\ S_1 + \left|\dot{\beta}_2\right|\ S_2 + \left|\dot{\beta}_3\right|\ S_3 + J_\chi\left(B_n\right) + J_f\left(X, Y, Z\right)\end{aligned} \tag{12}$$

From this pseudo-potential, it is possible to write the complementary equations to describe the internal variables evolution.

$$\dot{\beta}_i \in \frac{\partial\phi}{\partial B_i} \quad \dot{\varepsilon}_p \in \frac{\partial\phi}{\partial X} \quad \dot{\gamma} \in \frac{\partial\phi}{\partial Y} \quad \dot{\mu} \in \frac{\partial\phi}{\partial Z} \quad \dot{\varepsilon}_{tp} = \frac{\partial\phi}{\partial R} \quad \dot{\xi}_i = \frac{\partial\phi}{\partial S_i} \tag{13}$$

Concerning the previous equations, the parameters E, Ω, K and H are defined as a linear combination of their correspondent values for austenitic and martensitic phases, *i.e.*, $() = ()_M - \beta_3\left[()_M - ()_A\right]$. Besides, Λ_i depend linearly on temperature and are defined as: $\Lambda_i = \Lambda_i(T) = -L_0^{T,C,A} + \frac{L^{T,C,A}}{T_M}(T - T_M)$.

The parameters η_i are associated with the internal dissipation of the material, while η_{ci} and η_{ck} are (isotropic and kinematic, respectively) parameters related to plastic-phase transformation coupling. These parameters are determined as: $\eta_{ci,ck} = \bar{\eta}_{ci,ck}\exp\ \left[-m_p\ \left(\xi_1 + \xi_2\right)\right]$, where m_p is a saturation parameter and $\bar{\eta}_{ci}$ and $\bar{\eta}_{ck}$ give the magnitude of this coupling phenomenon.

In order to take into account differences on the kinetics of phase transformation for loading and unloading processes, it is possible to consider different values for the parameter η_i. Besides, J_χ is the indicator function related to the convex set χ, which provide constraints associated with phase transformations evolution, such as internal subloops due to incomplete phase transformations description and $M+ \Rightarrow M$ and $M-- \Rightarrow M$ phase transformations avoidance. For a mechanical loading history with $\dot{\sigma} \neq 0$, the convex set χ assumes the following form:

$$\chi = \left\{ \dot{\beta}_i \in \Re \;\middle|\; \begin{array}{lll} \dot{\varepsilon}\,\dot{\beta}_1 \geq 0; & \dot{\varepsilon}\,\dot{\beta}_3 \leq 0 & \text{if } \varepsilon_0 > 0 \\ \dot{\varepsilon}\,\dot{\beta}_2 \leq 0; & \dot{\varepsilon}\,\dot{\beta}_3 \geq 0 & \text{if } \varepsilon_0 < 0 \end{array} \right\} \tag{14}$$

On the other hand, when $\dot{\sigma} = 0$, the convex set χ is expressed by:

$$\chi = \left\{ \dot{\beta}_i \in \Re \;\middle|\; \begin{array}{l} \dot{T}\,\dot{\beta}_1 \begin{cases} < 0 \text{ if } \dot{T} > 0\,,\ \sigma < \sigma_M^{Tcrit} \text{ and } \beta_1^s \neq 0 \\ = 0 \text{ otherwise} \end{cases} ; \\ \dot{T}\,\dot{\beta}_2 \begin{cases} < 0 \text{ if } \dot{T} > 0\,,\ \sigma < \sigma_M^{Ccrit} \text{ and } \beta_2^s \neq 0 \\ = 0 \text{ otherwise} \end{cases} ; \\ \dot{T}\,\dot{\beta}_3 \geq 0 \\ -\dot{\beta}_1^2 - \dot{\beta}_1\dot{\beta}_3 = 0 \quad \text{or} \quad -\dot{\beta}_2^2 - \dot{\beta}_2\dot{\beta}_3 = 0 \end{array} \right\} \tag{15}$$

where β_1^s and β_2^s are the values of β_1 and β_2, respectively, when the phase transformation begins to take place. Moreover, the quantities ε_0 (created to discard the thermal expansion/contraction effect, while evaluating stress induced transformations) and σ_M^{Tcrit} and σ_M^{Ccrit} (which are the critical stress values for $M \Rightarrow M+$ and $M \Rightarrow M--$ phase transformations) can be analytically obtained [16] and give the following expressions:

$$\varepsilon_0 = \varepsilon - \frac{\Omega}{E}(T - T_0) \tag{16}$$

$$\sigma_M^{Tcrit} = \frac{E_M}{\alpha^T + E_M\alpha_h^T}\left[L_0^T - \frac{L^T(T-T_M)}{T_M} + \alpha_h^T\Omega_M(T-T_0) + \eta_{ci}K_M\gamma + \eta_{ck}\frac{\mu}{H_M}\right] - \Omega_M(T-T_0) \tag{17}$$

$$\sigma_M^{Ccrit} = \frac{E_M}{\alpha^C + E_M\alpha_h^C}\left[-L_0^C + \frac{L^C(T-T_M)}{T_M} + \alpha_h^C\Omega_M(T-T_0) - \eta_{ci}K_M\gamma - \eta_{ck}\frac{\mu}{H_M}\right] - \Omega_M(T-T_0) \tag{18}$$

Moreover, it is worthwhile to define the parameters α_h^T and α_h^C that help control the horizontal width of stress induced hysteresis loop.

$$\alpha_h^T = \varepsilon_R^T - \frac{\alpha^T}{E_M} - \frac{\Omega_M}{E_M}\left(T_C^T - T_0\right) \quad \alpha_h^C = -\varepsilon_R^C - \frac{\alpha^C}{E_M} + \frac{\Omega_M}{E_M}\left(T_C^C - T_0\right) \tag{19}$$

The other indicator function (J_f) is related to the yield surface defined as follows:

$$f = |X + HZ| - (\sigma_Y - Y) \tag{20}$$

The yield limit σ_Y has different values for austenitic and martensitic phases. Moreover, for very high temperatures, this value tends to decrease. Therefore, it is assumed that the yield limit has a linear variation with T, where T_F is a reference temperature related to high values of temperature.

These equations form a complete set of constitutive equations. Since the pseudo-potential of dissipation is convex, positive and vanishes at the origin, the Clausius-Duhen inequality is automatically satisfied if the entropy is defined as $s = -\partial\psi/\partial T$. Box 1 summarizes the set of constitutive equations for the proposed model. In this Box, notice that $\partial_{\beta_i}J_\pi$ are the sub-differentials with respect to β_i; λ is the plastic multiplier and $\partial_{\dot{\beta}_i}J_\chi$ are the sub-differentials with respect to variables $\dot{\beta}_i$.

Box 1. Constitutive equations.

$$
\begin{aligned}
&\sigma = E\left(\varepsilon - \varepsilon_p - \varepsilon_{tp} + \alpha_h^C \beta_2 - \alpha_h^T \beta_1\right) + \alpha^C \beta_2 - \alpha^T \beta_1 - \Omega\,(T - T_0)\\
&\dot{\beta}_1 = \frac{1}{\eta_1}\Big\{\alpha^T(\varepsilon - \varepsilon_p - \varepsilon_{tp}) + \Lambda_1 + \beta_2\left(\alpha_h^C \alpha^T + \alpha_h^T \alpha^C + E\alpha_h^T \alpha_h^C\right) - \beta_1\left(2\,\alpha_h^T \alpha^T + E\,\alpha_h^{T^2}\right) +\\
&\qquad + \alpha_h^T\left[E\,(\varepsilon - \varepsilon_p - \varepsilon_{tp}) - \Omega\,(T - T_0)\right] - \eta_{ci} K\gamma - \eta_{ck}\frac{\mu}{H} - \partial_{\beta_1} J_\pi\Big\} + \partial_{\dot{\beta}_1} J_\chi\\
&\dot{\beta}_2 = \frac{1}{\eta_2}\Big\{-\alpha^C\,(\varepsilon - \varepsilon_p - \varepsilon_{tp}) + \Lambda_2 + \beta_1\left(\alpha_h^T \alpha^C + \alpha_h^C \alpha^T + E\alpha_h^C \alpha_h^T\right) - \beta_2\left(2\,\alpha_h^C \alpha^C + E\,\alpha_h^{C^2}\right) -\\
&\qquad - \alpha_h^C\left[E\,(\varepsilon - \varepsilon_p - \varepsilon_{tp}) - \Omega\,(T - T_0)\right] - \eta_{ci} K\gamma - \eta_{ck}\frac{\mu}{H} - \partial_{\dot{\beta}_2} J_\pi\Big\} + \partial_{\dot{\beta}_2} J_\chi\\
&\dot{\beta}_3 = \frac{1}{\eta_3}\Big\{-\frac{1}{2}\,(E_A - E_M)\left(\varepsilon - \varepsilon_p - \varepsilon_{tp} + \alpha_h^C \beta_2 - \alpha_h^T \beta_1\right)^2 +\\
&\qquad + \Lambda_3 + (\Omega_A - \Omega_M)\,(T - T_0)\left(\varepsilon - \varepsilon_p - \varepsilon_{tp} + \alpha_h^C \beta_2 - \alpha_h^T \beta_1\right) -\\
&\qquad - \frac{1}{2}(K_A - K_M)\,\gamma^2 - \left(\frac{1}{2\,H_A} - \frac{1}{2\,H_M}\right)\mu^2 + \eta_{ci} K\gamma + \eta_{ck}\frac{\mu}{H} - \partial_{\dot{\beta}_3} J_\pi\Big\} + \partial_{\dot{\beta}_3} J_\chi\\
&\dot{\varepsilon}_p = \lambda\,\mathrm{sign}\,(\sigma - \mu) \qquad \dot{\gamma} = |\,\dot{\varepsilon}_p\,| + \eta_{ci}\left(\dot{\beta}_1 + \dot{\beta}_2 - \dot{\beta}_3\right) \qquad \dot{\mu} = H\,\dot{\varepsilon}_p + \eta_{ck}\left(\dot{\beta}_1 + \dot{\beta}_2 - \dot{\beta}_3\right)\\
&\dot{\varepsilon}_{tp} = 2\,\sigma\,\left[(M_{13}\beta_1 + M_{31}\beta_3)\,\dot{\beta}_1 + (M_{23}\beta_2 + M_{32}\beta_3)\,\dot{\beta}_2\right] + \left[M_{34}\beta_3 + M_{43}\,(1 - \beta_1 - \beta_2 - \beta_3)\right]\,\dot{\beta}_3\\
&\dot{\xi}_1 = \left|\,\dot{\beta}_1\,\right| \qquad \dot{\xi}_2 = \left|\,\dot{\beta}_2\,\right| \qquad \dot{\xi}_3 = \left|\,\dot{\beta}_3\,\right|
\end{aligned}
$$

The solution of the constitutive equations employs an *implicit Euler method* together with the *operator split technique* [19]. For β_n $(n = 1,2,3)$ calculation, the evolution equations are solved in a decoupled way. At first, the equations (except for the sub-differentials) are solved using an iterative *implicit Euler method*. If the estimated results obtained for β_n does not fit the imposed constraints, an *orthogonal projection algorithm* pulls their value to the nearest point on the domain's surface. For details, see [16].

3 Numerical simulations

In this section, some SMA behaviors are presented considering results obtained from the proposed model. In each of the following examples, whenever a phenomenon is not focused on, for the sake of simplicity, the related parameters are omitted.

At first, pseudoelastic behavior is focused on comparing numerical simulation with experimental data presented by [20], which describes tensile tests on Ni-Ti wires at different temperatures. Basically, three different temperatures are considered: 333K, 353K and 373K. Temperature T= 373K is used to calibrate model parameters, in order to reproduce the experimental data. Table 1 presents the adjusted model parameters. Figure 1 establishes a comparison between numerical results with those obtained from experimental tests showing that they are in close agreement for these temperatures.

Since neither the TRIP phenomenon is considered, nor the yielding surface is reached, numerical results do not present plastic strains upon unloading.

Table 1: Model parameters for pseudoelastic tests of a Ni-Ti SMA, without TRIP ([16, 20]).

E_A (GPa)	E_M (GPa)	Ω_A (MPa/K)	Ω_M(MPa/K)	α^T (MPa)	ε_R^T
54	42	0.74	0.17	330	0.0555
L_0^T (MPa)	L^T (MPa)	L_0^A (MPa)	L^A (MPa)	T_M (K)	T_A (K)
0.15	41.5	0.63	185	292	323
η_1^L (MPa.s)	η_1^U (MPa.s)	η_3^L (MPa.s)	η_3^U (MPa.s)	T_0 (K)	
1	2.7	1	2.7	298	

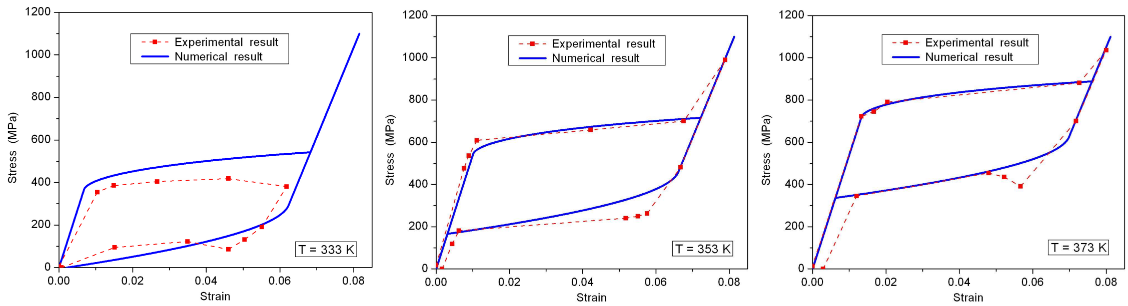

(a) (b) (c)

Figure 1: Comparison between numerical results provided by the model (without considering TRIP phenomenon) and experimental results by [20] for pseudoelastic behavior for three different temperatures. (a) $T = 333$ K; (b) $T = 353$ K and (c) $T = 373$ K.

Transformation Induced Plasticity (TRIP) is widely defined in the literature as the plastic flow arising from solid state phase transformation processes involving volume and/or shape changes without overlapping the yield surface [21]. At this point, TRIP phenomenon is focused on in order to reproduce the residual strain present at the experimental tests of [20], discussed in the previous example. The parameters used to obtain these results are listed in Table 2. Figure 2 brings the comparison between experimental and numerical results for pseudoelastic tests at three different temperatures now including TRIP phenomenon. Notice that, for the two highest temperatures, there is an amount

Table 2: Model parameters for pseudoelastic tests of a Ni-Ti SMA, including TRIP ([17, 20]).

E_A (GPa)	E_M (GPa)	Ω_A (MPa/K)	Ω_M(MPa/K)	α^T (MPa)	ε_R^T	L_0^T (MPa)
60	40	0.74	0.17	755	0.0517	5
L^T (MPa)	L_0^A (MPa)	L^A (MPa)	$\bar{M}_{13}$ (GPa^{-1})	$\bar{M}_{31}$ (GPa^{-1})	η_1^L (MPa.s)	η_1^U (MPa.s)
161	10	300	0.013	0.013	1.8	0.95
η_3^L (MPa.s)	η_3^U (MPa.s)	$\bar{M}_{34}$	$\bar{M}_{43}$	T_M (K)	T_0 (K)	T_A (K)
1.8	0.68	0	0	292	298	323
T_{TRIP} (K)	T_F (K)	m_1	m_3	m_p		
333	423	0.2	0.2	0.1		

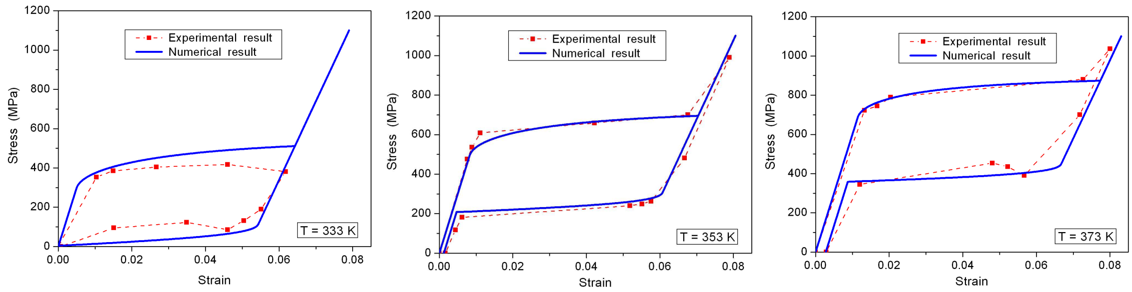

(a) (b) (c)

Figure 2: Comparison between numerical results provided by the model (considering TRIP phenomenon) and experimental results by [20] for pseudoelastic behavior for three different temperatures. (a) $T = 333$ K; (b) $T = 353$ K and (c) $T = 373$ K.

of irreversible strain, which is not recovered. Moreover, TRIP effect tends to decrease with decreasing temperature until it vanishes for $T = T_{TRIP} = 333$K. Again, it should be pointed out the close agreement between numerical and experimental results.

The hysteretic response of SMAs is one of their essential characteristics and it is possible to say that the major (or external) hysteresis loop can be defined as the envelope of all minor (or internal) hysteresis loops, usually denoted as subloops. At this point, a comparison between numerical results provided by the model and experimental results presented by [22] is presented in Figure 3, attesting the model capability of describing internal subloops. Parameters used to obtain these results are listed in Table 3. The experimental result describes tensile tests on Ni-Ti wires subjected to isothermal non-proportional mechanical loading that result in incomplete phase transformations.

Experimental results had shown that SMAs present an asymmetric behavior when subjected to tensile or compressive loads. For example, NiTi SMAs deformed under compression present smaller

Table 3: Model parameters for subloops test of a NI-Ti SMA ([18, 22]).

E_A (GPa)	E_M (GPa)	Ω_A (MPa/K)	Ω_M(MPa/K)	α^T (MPa)	ε_R^T
6.5	4.65	0.74	0.17	1.95	0.052
L_0^T (MPa)	L^T (MPa)	L_0^A (MPa)	L^A (MPa)	T_M (K)	η_1^L (MPa.s)
36.83	230	20	180	263	89.6
η_1^U (MPa.s)	η_3^L (MPa.s)	η_3^U (MPa.s)	T_0 (K)		
77.5	89	77	378		

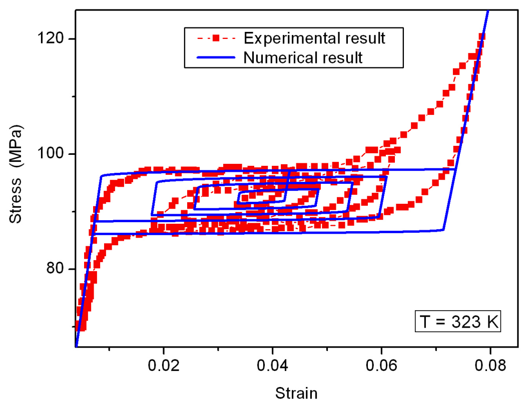

Figure 3: Comparison between numerical result provided by the model and experimental result by [22] for pseudoelastic subloops.

Table 4: Model parameters for tensile-compressive asymmetry test of an over-aged NiTi single crystal ([16, 23]).

E_A (GPa)	E_M (GPa)	α^T (MPa)	α^C (MPa)	ε_R^T	ε_R^C
94	161	2250	1670	0.0723	-0.0311
L_0^T (MPa)	L^T (MPa)	L_0^C (MPa)	L^C (MPa)	L_0^A (MPa)	L^A (MPa)
12.51	209.55	9.5	300.25	13.34	456
η_1^L (MPa.s)	η_1^U (MPa.s)	η_2^L (MPa.s)	η_2^U (MPa.s)	η_3^L (MPa.s)	η_3^U (MPa.s)
1.91	1.91	2.063	2.063	2	2
Ω_A (MPa/K)	Ω_M(MPa/K)	T_M (K)	T_A (K)	T_0 (K)	
0.74	0.17	271.2	301.7	295	

recoverable strain levels, higher critical transformation stress levels, and steeper transformation stress-strain slopes, no matter whether they are single or polycrystalline [23]. In Figure 4, comparisons between numerical results provided by the proposed model with experimental results by [23] for a single crystal Ni-Ti SMA pre-heat treated over-aged 1.5h at 673K show a close agreement. Both tensile and compressive tests are performed at a constant temperature. Table 4 presents the parameters related to both tests.

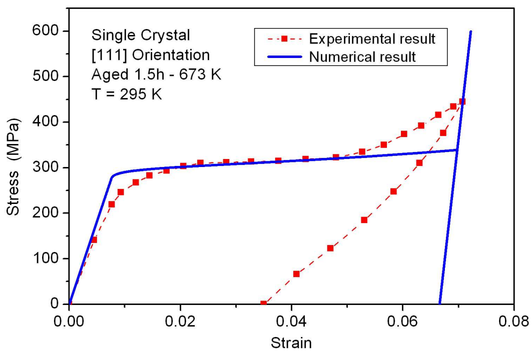

(a)

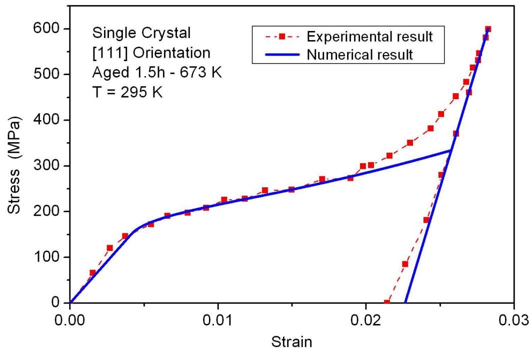

(b)

Figure 4: Comparison between numerical results provided by the model and experimental results by [23] for tensile-compressive asymmetry. (a) Tensile test; (b) Compressive test.

A nine-cycle thermomechanical loading process is now considered in order to show some features related to thermal, plastic and phase transformations behaviors. Each complete cycle consists of a high temperature isothermal mechanical loading/unloading cycle that overlaps the yielding limit followed by a cooling/heating thermal cycle. Since the test is performed at a high temperature, no stress induced transformation occurs and only plastic behavior takes place. SMA parameters employed on this numerical simulation are presented in Table 5. Figure 5 shows a stress-strain curve related to the mechanical cycle, presenting linear hardening classical plasticity. Figure 6 illustrates the strain-temperature response where it is possible to identify a thermal hysteresis loop. These results are in qualitative agreement with experimental data presented by [24], where it should be highlighted that the cumulative plastic strains tend not only to alter the phase transformation temperature but also to enlarge hysteresis loops. This behavior is closely related to the two-way shape memory effect. For more details, see [14] and [24].

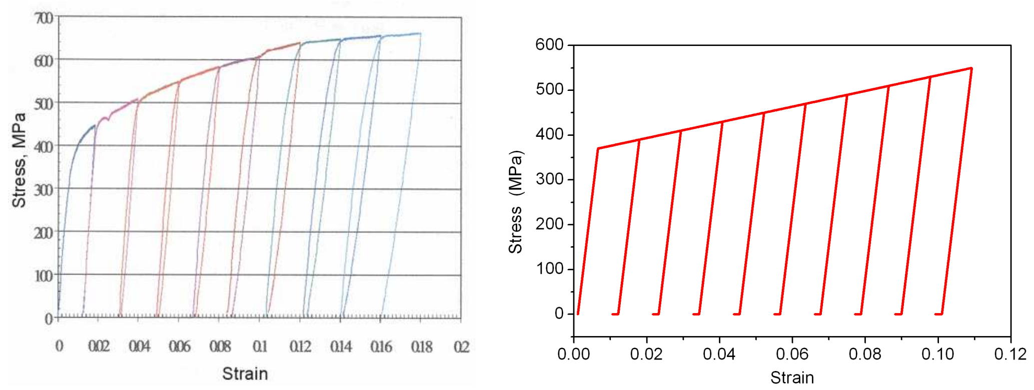

(a) (b)

Figure 5: Stress-strain diagram for qualitative comparison between numerical results provided by the model and experimental results by [24] for cyclic test to verify plastic-phase transformation coupling. (a) Experimental result; (b) Numerical result.

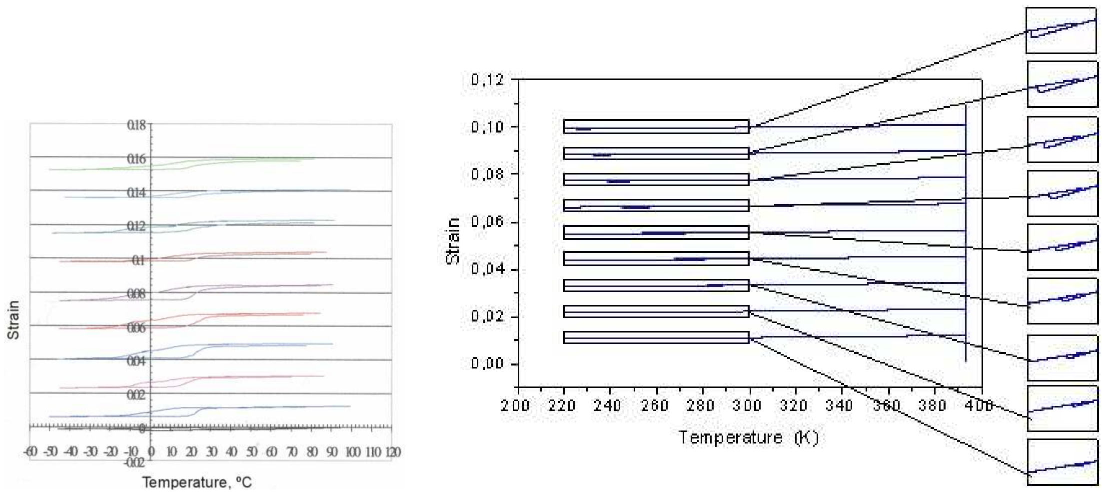

(a) (b)

Figure 6: Strain-temperature diagram for qualitative comparison between numerical results provided by the model and experimental results by [24] for cyclic test to verify plastic-phase transformation coupling. (a) Experimental result; (b) Numerical result.

Table 5: Model parameters for cyclic test to verify plastic-phase transformation coupling on NiTi SMA ([14, 24, 25]).

E_A (GPa)	E_M (GPa)	Ω_A (MPa/K)	Ω_M(MPa/K)	α^T (MPa)	ε_R^T	L_0^T (MPa)
67	26.3	0.74	0.17	89.42	0.067	0
L^T (MPa)	L_0^A (MPa)	L^A (MPa)	T_M (K)	T_0 (K)	η_1^L (MPa.s)	η_1^U (MPa.s)
212	0	200	292	298	0.07	0.04
η_3^L (MPa.s)	η_3^U (MPa.s)	T_A (K)	T_F (K)	K_A (GPa)	K_M (GPa)	H_A (GPa)
0.07	0.04	307	423	1.4	0.4	0.4
H_M (GPa)	η_{ci}	η_{ck}	σ_Y^M (MPa)	$\sigma_Y^{A,i}$ (MPa)	$\sigma_Y^{A,f}$ (MPa)	
0.11	0.02	0.02	200	690	257.72	

4 Conclusions

The present contribution discusses the phenomenological modeling of shape memory alloys presenting a one-dimensional constitutive model. The proposed model is able to capture the general thermo-mechanical behavior of SMAs, including pseudoelasticity, shape memory effect, phase transformation due to temperature variation, internal subloops due to incomplete phase transformations, plasticity, plastic-phase transformation coupling and transformation induced plasticity. A comparison between numerical simulations and experimental tests show that these results are in close agreement. Although each phenomenon is treated isolated in this paper (in order to compare with available data in the literature), the model is able to describe all these phenomena together, which confer a great flexibility to the model use.

Acknowledgements

The authors acknowledge the support of the *Brazilian Research Council (CNPq)*.

References

[1] Duerig, T., Pelton, A. & Stöckel, D., An overview of nitinol medical applications. *A Materials Science and Engineering*, **273-275**, pp. 149–160, 1999.
[2] Machado, L. & Savi, M., Medical applications of shape memory alloys. *Brazilian Journal of Medical and Biological Research*, **36(6)**, pp. 683–691, 2003.
[3] van Humbeeck, J., Non-medical applications of shape memory alloys. *A Materials Science and Engineering*, **273-275**, 1999.
[4] Lagoudas, D., Rediniotis, O. & Khan, M., Applications of shape memory alloys to bioengineering and biomedical technology. *4th International Workshop on Mathematical Methods in Scattering Theory and*

Biomedical Technology, Perdika - Greece, 1999.
[5] Paiva, A. & Savi, M., An overview of constitutive models for shape memory alloys. *Mathematical Problems in Engineering*, **2006(ID56876)**, pp. 1–30, 2006.
[6] Denoyer, K., Erwin, R. & Ninneman, R., Advanced smart structures flight experiments for precision spacecraft. *Acta Astronautica*, **47**, pp. 389–397, 2000.
[7] XIV the Brazilian Congress of Mechanical Engineering (COBEM 97 - ABCM), *A Non-Explosive Release Device for Aerospace Applications using Shape Memory Alloys*, PMCL Pacheco and MA Savi.
[8] L.J.Garner, L.N.Wilson, D.C.Lagoudas & Rediniotis, O., Development of a shape memory alloy actuated biomimetic vehicle. *Smart Materials & Structures*, **9(5)**, pp. 673–683, 2001.
[9] Webb, G., Wilson, L., Lagoudas, D. & Rediniotis, O., Adaptive control of shape memory alloy actuators for underwater biomimetic applications. *AIAA Journal*, **38(2)**, pp. 325–334, 2000.
[10] Rogers, C., Intelligent materials. *Scientific American*, pp. 122–127, 1995.
[11] Birman, V., Theory and comparison of the effect of composite and shape memory alloy stiffeners on stability of composite shells and plates. *International Journal of Mechanical Sciences*, **39(10)**, pp. 1139–1149, 1997.
[12] Fremond, M., Matériaux à mémoire de forme. *CR Acad Sc Paris Tome*, **304(7)**, pp. 239–244, 1987.
[13] Fremond, M., Shape memory alloy: A thermomechanical macroscopic theory. *CISM Courses and Lectures*, **351**, pp. 3–68, 1996.
[14] Savi, M., Paiva, A., Baêta-Neves, A. & Pacheco, P., Phenomenological modeling and numerical simulation of shape memory alloys: A thermo-plastic-phase transformation coupled model. *Journal of Intelligent Material Systems and Structures*, **13(5)**, pp. 261–273, 2002.
[15] Baêta-Neves, A., Savi, M. & Pacheco, P., On the fremond's constitutive model for shape memory alloys. *Mechanics Research Communications*, **31(6)**, pp. 677–688, 2004.
[16] Paiva, A., Savi, M., Braga, A. & Pacheco, P., A constitutive model for shape memory alloys considering tensile-compressive asymmetry and plasticity. *International Journal of Solids and Structures*, **42(11-12)**, pp. 3439–3457, 2005a.
[17] Paiva, A., Savi, M. & Pacheco, P., Modeling transformation induced plasticity in shape memory alloys. *XVIII International Brazilian Congress of Mechanical Engineering - COBEM 2005*, 2005b.
[18] Savi, M. & Paiva, A., Describing internal subloops due to incomplete phase transformations in shape memory alloys. *Archive of Applied Mechanics*, **74(9)**, pp. 637–647, 2005.
[19] Ortiz, M., Pinsky, P. & Taylor, R., Operator split methods for the numerical solution of the elastoplastic dynamic problem. *Computer Methods of Applied Mechanics and Engineering*, **39**, pp. 137–157.
[20] Tobushi, H., Iwanaga, N., Tanaka, K., Hori, T. & Sawada, T., Deformation behavior of ni-ti shape memory alloy subjected to variable stress and temperature. *Continuum Mechanics and Thermodynamics*, **3**, pp. 79–93.
[21] Lagoudas, D., Entchev, P. & Kumar, P., (eds.), *Thermomechanical Characterization SMA Actuators Under Cyclic Loading*, IMECE'03 - 2003 ASME International Mechanical Engineering Congress: Washington D.C., 2003.
[22] Muller, I. & Xu, H., On the pseudo-elastic hysteresis. *Acta Metallurgical Materials*, **39(3)**, pp. 263–271, 1991.
[23] Gall, K., Sehitoglu, H., Chumlyakov, Y. & Kireeva, I., Tension-compression asymmetry of the stress-strain response in aged single crystal and polycrystalline niti. *Acta Mater*, **47(4)**, pp. 1203–1217, 1999.
[24] Miller, D. & Lagoudas, D., Thermo-mechanical characterization of niticu and niti sma actuators: Influence of plastic strains. *Smart Materials & Structures*, **5**, pp. 640–652, 2000.
[25] Paiva, A., *Modelagem do Comportamento Termomecânico das Ligas com Memória de Forma*. Ph.D.

thesis, Departament of Mechanical Engineering - Pontifícia Universidade Católica do Rio de Janeiro, Rio de Janeiro - Brazil, 2004.

Brazilian Society of Mechanical Sciences and Engineering, ISBN 978-85-85769-30-7